Article

Transport and field emission properties of MoS_2 bilayers

Francesca Urban[1,3], Maurizio Passacantando[2], Filippo Giubileo[3], Laura Iemmo[1,3], and Antonio Di Bartolomeo[1,3,*]

[1] Department of Physics "E.R. Caianiello", University of Salerno, 84084, Fisciano, Italy; furban@unisa.it, liemmo@unisa.it, adibartolomeo@unisa.it
[2] Department of Physical and Chemical Sciences, University of L'Aquila, and CNR-SPIN L'Aquila, 67100, L'Aquila, Italy; maurizio.passacantando@aquila.infn.it
[3] CNR-SPIN Salerno, 84084, Fisciano, Italy; filippo.giubileo@spin.cnr.it
* Correspondence: adibartolomeo@unisa.it; Tel.: +39-089-969-189

Abstract: We report the electrical characterization and the field emission properties of CVD-grown MoS_2 bilayers deposited on SiO_2/Si substrate. Current-voltage characteristics are measured in the back-gate transistor configuration, with Ti contacts patterned by electron beam lithography. We confirm the *n*-type character of as-grown MoS_2 and we report normally-on field effect transistors. Local characterization of field emission is performed inside a scanning electron microscope chamber with piezo-controlled tungsten tips working as the anode and the cathode. We demonstrate that an electric field of $\sim 200\, V/\mu m$ is able to extract current from the flat part of MoS_2 bilayers, which therefore can be conveniently exploited for field emission applications even in low field-enhancement configurations. We show that a Fowler-Nordheim model, modified to account for electron confinement in 2D materials, fully describes the emission process.

Keywords: Transition metal dichalcogenides, MoS_2, field effect transistor, field emission.

1. Introduction

Over the past decade, graphene and graphene-like materials have attracted a lot of attention. Due to the two-dimensional (2D) nature and several extraordinary properties, such as high mobility and current carrying capability, chemical stability and mechanical robustness, graphene in particular has been the most chosen material for new electronic devices [1,2]. However, the absence of an intrinsic bandgap has hampered its application as transistor channel [3,4] and has paved the way for the study of alternative 2D materials, with semiconducting behavior, such as the transition metal dichalcogenides (TMDs) [5,6]. The TMDs family, which comprises MX_2 compounds where M is a transition metal (Mo, W, etc.) and X a chalcogen (S, Se, Te), is gaining popularity in the scientific and engineering research. In particular, molybdenum disulfide (MoS_2) is intensively studied for the ease of fabrication and the direct bandgap suitable for optoelectronic applications [7–10].

Similarly to graphene, MoS_2 can be mechanically exfoliated from a bulk material and transferred on a substrate [6]; however, single-crystal and large-scale flakes, with controlled number of layers, are more easily produced by chemical vapor deposition (CVD) [11]. MoS_2 presents a structure consisting of a hexagonal plane of Mo atoms sandwiched between two planes of S atoms. Each layer is bonded to another one by van der Waals interactions to form the bulk structure. MoS_2 is considered a good candidate for electronic and optoelectronic applications because it offers control on the width of the energy bandgap through the number of layers [12], even though its mobility is typically only few tens $cm^2V^{-1}s^{-1}$ [8]. Indeed, multi-layers MoS_2 shows an indirect bandgap of 1.2 eV which increases with the decreasing number of layers and becomes direct and of $1.8 - 1.9\, eV$ for mono-layers. The presence of an energy gap enables MoS_2 transistors with high on/off ratio ($> 10^7$) [13] and low subthreshold swing (below $70\, mV/decade$) [14]; moreover, a field effect mobility

of about $200\ cm^2V^{-1}s^{-1}$ has been experimentally achieved [15]. Additional features, such as high photoresponsivity [10,16] and spin-orbit splitting [17], have been investigated, opening the route for applicability of MoS_2 for optoelectronic and spintronic devices [10,18].

In this paper, we characterize the transport properties of bilayer MoS_2 field effect transistors (FET) in the back-gate configuration. Furthermore, taking advantage of contacted MoS_2 flakes, we investigate their local field emission behavior.

Field emission (FE) is a quantum mechanical phenomenon in which electrons, extracted from a conductor or a semiconductor surface upon application of an intense electric field, flow in vacuum from a cathode to an anode. Classic field emission theory was developed by Fowler and Nordheim [19] for planar electrodes, but it is usually applied also to electrodes forming sharp tips [20]. Actually, tips with small radius of curvature enable enhancement of the local electric field, thereby requiring a reduced anode-to-cathode field for electron extraction [21]. Nanostructures, such as nanoparticles [22,23], nanowires [24] and nanotubes [21,25–28] or 2D materials [29,30], for their intrinsically sharp edges and high aspect ratio, are natural field emission sources. Indeed, semiconducting or metallic nanostructured materials have been considered for FE applications in vacuum electronics [31], flat panel displays [32], electron microscopy [33], x-ray tubes [34,35], etc.

To date, FE from MoS_2 has been very poorly characterized. There are few works concerning field emission measurements on MoS_2 nanostructures, like single and multi-layers flake, nanoflowers and films with edge terminated vertically aligned (ETVA)[36]. It has been also reported that ultra-thin ETVA-MoS_2 films present FE characteristics comparable to those of carbon-based structures [37–39].

Here, we measure FE current from the flat part of MoS_2 bilayers at a turn on field of $230\ V/\mu m$. Despite we operate under no field-enhancement condition, we find a local electric field magnified by a factor 10 at the cathode-anode distance $d = 75\ nm$ and that the field amplification factor increases linearly with d. Remarkably, we show that FE from MoS_2 bilayers follows a modified Fowler-Nordheim (FN) model recently proposed to include the effect of the confinement in 2D materials [40]. We highlight that, to the best of our knowledge, field emission from MoS_2 bilayers has not been reported before. Our study, demonstrating its suitability as field emitter, aims at exploiting MoS_2 in vacuum electronics, thus extending its use as electrode in heterojunctions and channel in field effect transistors.

2. Materials and Methods

The MoS_2 flakes were grown by CVD at $750\ K$ (using S and MoO_3 as precursors) on p-doped Si substrate covered by $300\ nm$ of SiO_2. The process yielded mainly bilayers and multilayers randomly distributed on the substrate. From scanning electron microscope (SEM) imaging, we often found traces of unreacted MoO_3 precursor on the flake, as shown in figure 1(a), which displays a typical back-gated field effect transistor with Ti/Au metal leads. Such residuals can affect the carrier mobility. A schematic of the device, consisting of a TLM structure (Transfer Length Method) with back gate, is reported in figure 1(b).

We use the silicon substrate as common back gate and metal leads, patterned by standard electron beam lithography and lift-off process, as drain and source. Metal leads are made of Ti ($20\ nm$) and Au ($130\ nm$) deposited as contact and cover layers, respectively.

MoS_2 flakes are characterized by Raman spectroscopy before the device fabrication in order to identify the number of layers. The Raman spectrum reported in figure 1(c), shows two identifying peaks: A_{1g} associated with the out-of-plane vibration of sulfur atoms and E^1_{2g} resulting from the in-plane vibrations of Mo and S atoms [41]. The two peaks are separated by $21\ cm^{-1}$ indicating bilayer flakes.

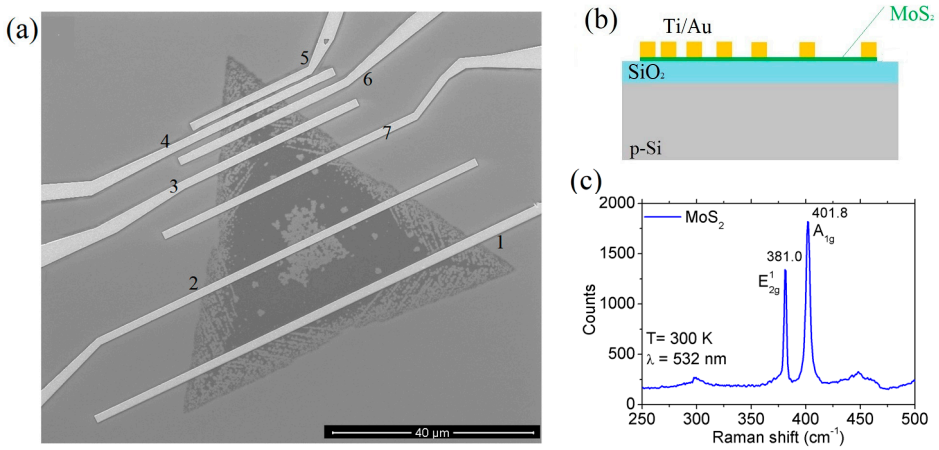

Figure 1. (a) SEM image of a Ti/Au contacted MoS_2 flake. (b) Schematic cross section of the field-effect device. (c) Raman spectrum of the flake.

In the following, the transistor characterization refers to contacts 4 (drain) and 5 (source), as marked in figure 1(a), i.e. to the device with the shortest-channel, which is the most interesting from an application perspective. The distance between the two contacts, i.e. the channel length, is $L = 0.57\ \mu m$, while the channel width is $W \sim 11.4\ \mu m$.

Electrical measurements are performed by a Keithley 4200 SCS (source-measurement unit) connected to a Janis ST-500 probe station at room temperature and pressure of $\sim 3\ mbar$.

Field emission measurements are carried out, at a pressure $< 10^{-6}\ mbar$, in a SEM vacuum chamber, endowed with two piezo-controlled tungsten tips (W-tips) with nanometric resolution.

3. Results

3.1 Transistor characterization

Figure 2 reports the electrical transport characterization of the back-gate MoS_2 transistor. The output characteristics $I_{ds} - V_{ds}$ (figure 2(a)) are measured from $-80\ V$ to $10\ V$, at gate voltage steps of $10\ V$. A channel resistance decrease, resulting in higher current, is observed for gate voltage, V_{gs}, varying from negative to positive voltages. This is further evidenced by the transfer $I_{ds} - V_{gs}$ characteristics, shown in figure 2(b) for a given drain-source bias voltage ($V_{ds} = 0.5\ V$).

The transfer curve discloses an n-type behavior, with normally-on channel at $V_{gs} = 0\ V$. The off-state of the transistor is reached below the negative gate voltage of $-80\ V$ that we safely adopted as lower limit for V_{gs} to prevent SiO_2 gate dielectric leakage or breakdown. The limited range of V_{gs} results in the apparent low on/off ratio of the transistor, which is essentially not turned off over the sweeping interval. Nevertheless, the measured portion of transfer curve is enough to estimate the threshold voltage. Being $I_{ds} \propto (V_{gs} - V_{th})$, the threshold voltage corresponds to the x-axis intercept of the straight-line fitting of the current in linear scale and results $V_{th} \sim -70\ V$. We calculate the subthreshold swing as $SS = dV_{gs}/d(logI_{ds})$=20 $V/decade$ using the transfer curve in logarithmic scale (blue curve). The high value of SS, which is likely overestimated due to the fitting region too close to V_{th}, is expected because of the low efficient back-gate configuration with thick gate oxide.

Remarkably, the prevailing on-state over a wide V_{gs} range and the n-type doping suggest that the MoS_2 flake can be suitable for electron extraction, i.e. for field emission applications.

Preprints (www.preprints.org) | NOT PEER-REVIEWED | Posted: 11 February 2018 doi:10.20944/preprints201802.0080.v1

Peer-reviewed version available at Nanomaterials 2018, 8, 151; doi:10.3390/nano8030151

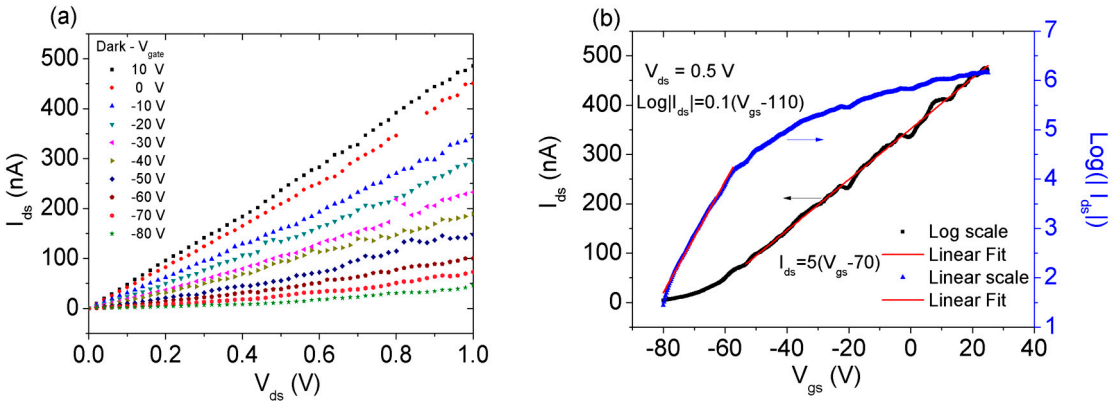

Figure 2. (a) Output characteristics $I_{ds} - V_{ds}$ of the MoS_2 transistor for different values of the gate bias V_{gs}. (b) Transfer characteristic $I_{ds} - V_{gs}$ (left scale) and $Log|I_{ds}| - V_{gs}$ (right scale) with linear fittings.

We also evaluate the field effect mobility from the slope of transfer characteristic (black curve) via the following formula

$$\mu = \frac{dI_{ds}}{dV_{gs}} \frac{L}{W \cdot C_{ox} \cdot V_{ds}}, \quad (1)$$

where $C_{ox} = \varepsilon_{ox}/d_{ox}$ is the oxide capacitance with ε_{ox} and d_{ox} the SiO_2 permittivity and thickness, respectively. $C_{ox} = 11\, nFcm^{-2}$ for $300\, nm\, SiO_2$ [42]. The obtained mobility, $0.046\, cm^2V^{-1}s^{-1}$, is on the low side of the range typically reported for uncovered MoS_2, ranging from $0.05\, cm^2V^{-1}s^{-1}$ to $100\, cm^2V^{-1}s^{-1}$ [8,31,43,44]. Our value of the field effect mobility could be slightly underestimated because it does not exclude the effect of the contact resistances [45], that increase the total resistance of the sample and the probability of electron scattering. The low mobility is caused by the mentioned process residues, the long exposure to air and the likely presence of defects in crystal structure.

3.2 Field emission measurements

FE experiment on a selected flake, shown in figure 3(a), has been performed inside the SEM chamber by placing one of the two available W-tips on the metal electrode contacting the flake (cathode) and positioning the other tip (anode) at a variable distance d from the flake, as displayed in figure 3(b).

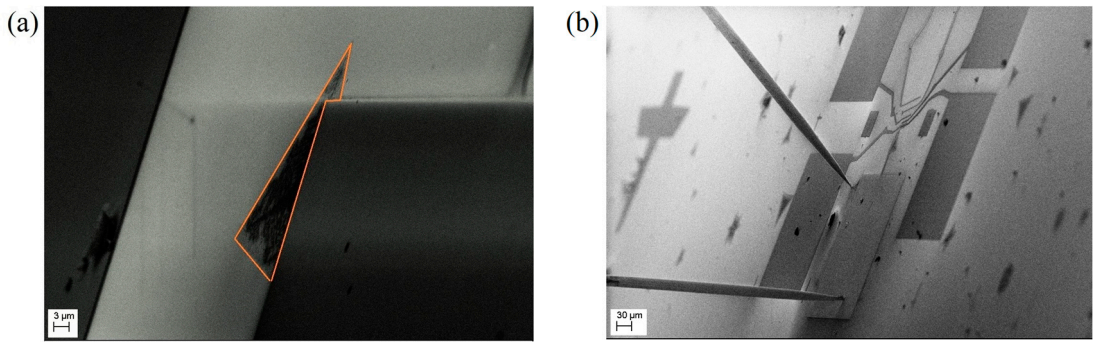

Figure 3. (a) SEM image of a MoS_2 flake used for field emission measurements. (b) SEM image showing the positioning of the tungsten tips: the lower W-tip is on the metal pad contacting the flake, the other one is placed in front of the flake at a close distance d.

Considering that the MoS_2 flake is n-doped and that the sharp edge originates a high electric field amplification, we expect easy extraction of electron from the edge of the flake upon application of a voltage. Nevertheless, exposure to air, flake oxidation and the higher concentration of process

Peer-reviewed version available at Nanomaterials 2018, 8, 151; doi:10.3390/nano8030151

145 residues at the edge, make it harder to extract electrons from the flake boundary. On the other hand,
146 due to a better surface quality (less contaminants) in the inner flat part of the flake, and taking
147 advantage from the fine positioning control of our W-tip, supported by SEM imaging, we have
148 performed field emission characterization from an internal, flat portion of the flake. FE from the flat
149 part of MoS_2 bilayers has not been reported in literature yet and constitutes an interesting way to
150 complete the on-going investigation on the field emission properties of MoS_2. Similarly, FE
151 measurements on graphene initially gave indication that emitting current was achievable only from
152 edges [46], but it was successively demonstrated that FE currents could be extracted from the inner
153 flat part of graphene flake under application of electric field of few hundreds $V/\mu m$ [47].
154 In figure 4(a) and 4(b), we show $I-V$ curves, in semi logarithmic and linear scale respectively,
155 at different anode-cathode distances (i.e. at variable separation between the W-tip and MoS_2
156 surface). The curves show the typical fluctuations of emission current, indicating desorption of
157 physisorbed molecules caused by Joule heating. Figure 4(a) shows that reducing the inter-electrodes
158 distance the field emission current appears at lower voltages, confirming that the FE turn-on voltage
159 depends on the electrode separation.
160 For a given distance, the current remains at the floor noise up to a threshold voltage,
161 corresponding to what we define as the FE turn-on voltage, above which it starts raising
162 exponentially up to $100\ nA$, as expected from Fowler-Nordheim (FN) theory. According to FN model

$$I = \frac{Sa\beta^2 E^2}{\Phi} \exp\left[-\frac{b\Phi^{\frac{3}{2}}}{\beta E}\right], \quad (2)$$

163 where a and b are constants with values $1.54 \cdot 10^{-6}\ A\ eV\ V^{-2}$ and $6.83 \cdot 10^{7}\ eV^{\frac{3}{2}}\ V\ cm^{-1}$
164 respectively, S and ϕ represent the emitting surface and the material work function (in our case $\phi =$
165 $5.25\ eV$ [48]), and β is the so-called field enhancement factor. β is a typical figure of merit for the
166 qualification of field emitting materials, despite it has been shown to depend on the experimental
167 setup [22]. Finally, the electric field is $E = V/d$, where V is the anode-cathode voltage.
168 The Fowler-Nordheim behavior of the field emission current is usually checked by the linearity
169 of the so-called FN plot of $\ln(I/V^2)$ vs $1/V$. In particular, the intercept and slope of the fitting
170 straight-line yield the emission area and the field enhancement factor β, respectively.
171 The FN plot of our measurements is reported in Figure 4(c), which confirms the expected linear
172 behavior. Figure 4(d) is the analogous of the FN plot for a modified Fowler-Nordheim model, recently
173 proposed by Yee Sin Ang et al. [40], to account for 2D electron confinement. This 2D FN model takes
174 into account that, differently from bulk materials, field emission from 2D materials may depend from
175 the extraction direction, and results in the following current-field equation
176

$$I_{FN}^{2D} = A_{FN}^{2D} \exp\left[-\frac{b\Phi^{\frac{3}{2}}}{\beta E}\right], \quad (3)$$

177 where A_{FN}^{2D} is a constant, and the other symbols are the same as in eq.(2). Figures 4(c) and 4(d) show
178 that both models well reproduce the experimental data. However, the 2D model provides a better fit
179 over a wider voltage range. Then, we use the 2D FN model for further analysis, and in particular to
180 evaluate the β at different distances d. The plot in figure 5(a) shows a linear behavior of $\beta(d)$ in
181 agreement with what has been often reported for different field emission sources [21,31,49,50]. Such
182 behavior is likely due the fact that at higher distance the field from the W-tip becomes more uniform
183 on the emitting area [51].

Preprints (www.preprints.org) | NOT PEER-REVIEWED | Posted: 11 February 2018 doi:10.20944/preprints201802.0080.v1

Peer-reviewed version available at Nanomaterials 2018, 8, 151; doi:10.3390/nano8030151

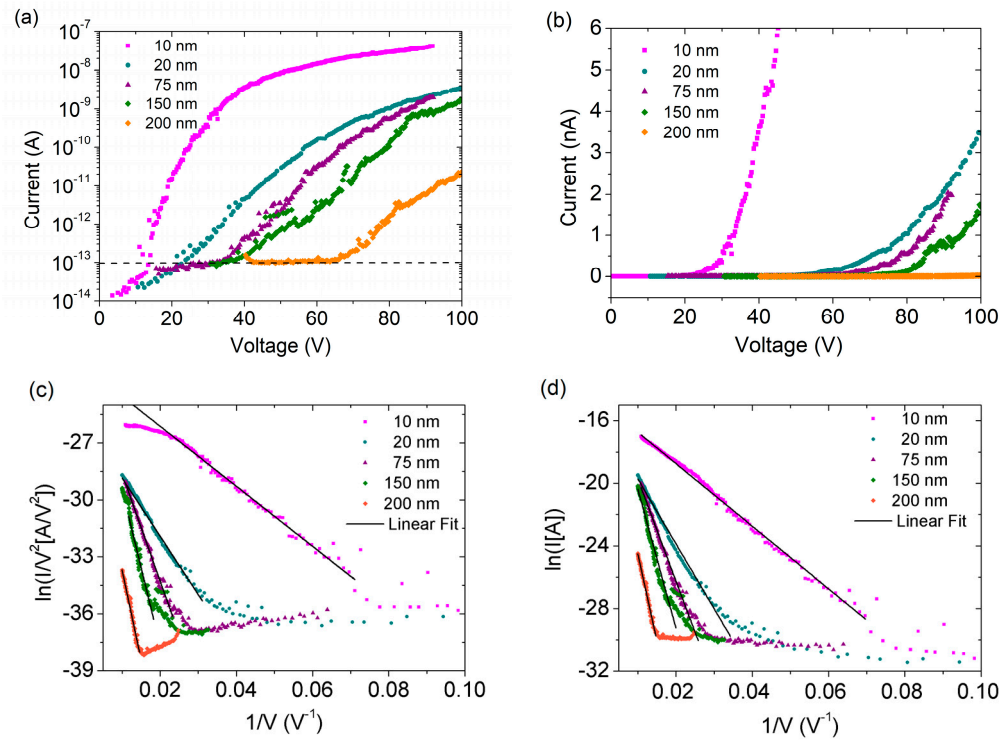

Figure 4. (a) Field emission current plotted as a function of applied voltage in semi logarithmic scale; the black line identifies the current level at which the turn on field is defined. (b) Field emission current plotted as a function of applied voltage in linear scale. (c) Experimental data plotted with 3D Fowler-Nordheim model. (d) Experimental data plotted with modified 2D Fowler-Nordheim model, showing good fit over a wider range.

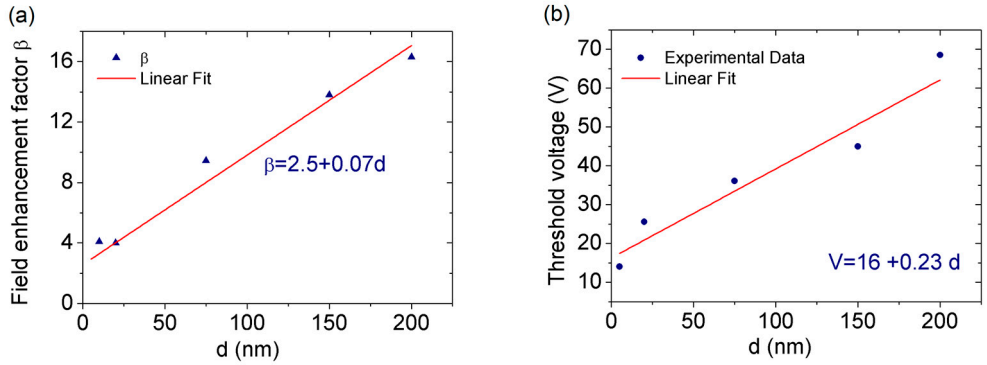

Figure 5. (a) Field enhancement factor as a function of the cathode-anode distance. (b) Threshold voltage as a function of cathode-anode distance.

The seemingly low value of the amplification factor, less than 20 for $d < 200\ nm$, is remarkable if we consider that emission happen from the inner part of the flake, where no field enhancement by edge effect takes place, and that β further increases with the distance d.

Finally, we can evaluate the turn-on field from the voltage values at which the current emerges from the noise floor of $1 \times 10^{-13} A$. From the slope of the fitting straight line of threshold voltage versus d plot, shown in figure 5 (b), we estimate the turn on field as $230\ V/\mu m$. If compared to the typical turn-on field of several $kV/\mu m$ needed to extract electrons from flat surfaces, the obtained turn-on field can be considered a good result, pointing to noteworthy, although still unexploited, FE capabilities of MoS_2.

4. Conclusion

We have presented the electrical transport characterization of field effect transistors with MoS_2 bilayers channel. The conductance shows an n-type behavior and gate modulation, with prevailing on-state over a wide voltage range. This feature has suggested the use of MoS_2 flake for field emission investigations. We have reported significant field emission from the flat part of the flake under the application of a moderate electric field, even without taking advantage from the field enhancement due to edge effects. We have also demonstrated that a modified field emission model, which considers the 2D nature of the flakes, provides a better fitting compared to traditional 3D Fowler-Nordheim theory. This study, demonstrating MoS_2 suitability as field emitter, is a step ahead towards the exploitation of MoS_2 for vacuum electronics applications, in addition to its established use as electrode in heterojunctions and channel in field effect transistors.

Acknowledgments: We acknowledge the economic support of POR Campania FSE 2014–2020, Asse III Ob. Specifico l4, Avviso pubblico decreto dirigenziale n. 80 del 31/05/2016.

Author Contributions: A.D.B., F.G. and M.P. conceived and designed the experiments; F.G., M.P. and L.I. performed the experiments; F.U., L.I. and A.D.B. analyzed the data; A.D.B., F.G. and M.P. contributed reagents/materials/analysis tools; F.U. and A.D.B. wrote the paper.

Conflicts of Interest: The authors declare no conflict of interest.

References

1. Schwierz, F. Graphene transistors. *Nature Nanotechnology* **2010**, *5*, 487.
2. Avouris, P. Graphene: Electronic and Photonic Properties and Devices. *Nano Letters* **2010**, *10*, 4285–4294, doi:10.1021/nl102824h.
3. Di Bartolomeo, A.; Giubileo, F.; Iemmo, L.; Romeo, F.; Santandrea, S.; Gambardella, U. Transfer characteristics and contact resistance in Ni- and Ti-contacted graphene-based field-effect transistors. *Journal of Physics: Condensed Matter* **2013**, *25*, 155303.
4. Di Bartolomeo, A.; Giubileo, F.; Romeo, F.; Sabatino, P.; Carapella, G.; Laura Iemmo; Schroeder, T.; Lupina, G. Graphene field effect transistors with niobium contacts and asymmetric transfer characteristics. *Nanotechnology* **2015**, *26*, 475202.
5. Zhou, Z.; Yap, Y. K. Two-Dimensional Electronics and Optoelectronics: Present and Future. *Electronics* **2017**, *6*, 53, doi:10.3390/electronics6030053.
6. Lin, Z.; McCreary, A.; Briggs, N.; Subramanian, S.; Zhang, K.; Sun, Y.; Li, X.; Borys, N. J.; Yuan, H.; Fullerton-Shirey, S. K.; Chernikov, A.; Zhao, H.; McDonnell, S.; Lindenberg, A. M.; Xiao, K.; LeRoy, B. J.; Drndić, M.; Hwang, J. C. M.; Park, J.; Manish Chhowalla; Schaak, R. E.; Javey, A.; Hersam, M. C.; Robinson, J.; Terrones, M. 2D materials advances: from large scale synthesis and controlled heterostructures to improved characterization techniques, defects and applications. *2D Materials* **2016**, *3*, 042001.
7. Di Bartolomeo, A.; Genovese, L.; Giubileo, F.; Iemmo, L.; Luongo, G.; Tobias Foller; Schleberger, M. Hysteresis in the transfer characteristics of MoS 2 transistors. *2D Materials* **2018**, *5*, 015014.
8. Yoon, Y.; Ganapathi, K.; Salahuddin, S. How Good Can Monolayer MoS2 Transistors Be? *Nano Letters* **2011**, *11*, 3768–3773, doi:10.1021/nl2018178.
9. Late, D. J.; Shaikh, P. A.; Khare, R.; Kashid, R. V.; Chaudhary, M.; More, M. A.; Ogale, S. B. Pulsed Laser-Deposited MoS2 Thin Films on W and Si: Field Emission and Photoresponse Studies. *ACS Applied Materials & Interfaces* **2014**, *6*, 15881–15888, doi:10.1021/am503464h.
10. Lopez-Sanchez, O.; Lembke, D.; Kayci, M.; Radenovic, A.; Kis, A. Ultrasensitive photodetectors based on monolayer MoS2. *Nature Nanotechnology* **2013**, *8*, 497.

11. Feng, Y.; Zhang, K.; Wang, F.; Liu, Z.; Fang, M.; Cao, R.; Miao, Y.; Yang, Z.; Mi, W.; Han, Y.; Song, Z.; Wong, H. S. P. Synthesis of Large-Area Highly Crystalline Monolayer Molybdenum Disulfide with Tunable Grain Size in a H2 Atmosphere. *ACS Applied Materials & Interfaces* **2015**, *7*, 22587–22593, doi:10.1021/acsami.5b07038.
12. Mak, K. F.; Lee, C.; Hone, J.; Shan, J.; Heinz, T. F. Atomically Thin MoS2: A New Direct-Gap Semiconductor. *Phys. Rev. Lett.* **2010**, *105*, 136805, doi:10.1103/PhysRevLett.105.136805.
13. Zhou, C.; Wang, X.; Raju, S.; Lin, Z.; Villaroman, D.; Huang, B.; Chan, H. L.-W.; Chan, M.; Chai, Y. Low voltage and high ON/OFF ratio field-effect transistors based on CVD MoS2 and ultra high-k gate dielectric PZT. *Nanoscale* **2015**, *7*, 8695–8700, doi:10.1039/C5NR01072A.
14. Nourbakhsh, A.; Zubair, A.; Joglekar, S.; Dresselhaus, M.; Palacios, T. Subthreshold swing improvement in MoS2 transistors by the negative-capacitance effect in a ferroelectric Al-doped-HfO2/HfO2 gate dielectric stack. *Nanoscale* **2017**, *9*, 6122–6127, doi:10.1039/C7NR00088J.
15. Radisavljevic, B.; Radenovic, A.; Brivio, J.; Giacometti, V.; Kis, A. Single-layer MoS2 transistors. *Nature Nanotechnology* **2011**, *6*, 147.
16. Di Bartolomeo, A.; Genovese, L.; Foller, T.; Giubileo, F.; Luongo, G.; Luca Croin; Liang, S.-J.; Ang, L. K.; Schleberger, M. Electrical transport and persistent photoconductivity in monolayer MoS 2 phototransistors. *Nanotechnology* **2017**, *28*, 214002.
17. Zibouche, N.; Kuc, A.; Musfeldt, J.; Heine, T. Transition-metal dichalcogenides for spintronic applications. *Annalen der Physik* **2014**, *526*, 395–401, doi:10.1002/andp.201400137.
18. Han, W. Perspectives for spintronics in 2D materials. *APL Materials* **2016**, *4*, 032401, doi:10.1063/1.4941712.
19. Fowler, R. H.; Nordheim, L. Electron emission in intense electric fields. *Proc R Soc London A* **1928**, *119*, 173–181, doi:10.1098/rspa.1928.0091.
20. C. A. Spindt; C. E. Holland; A. Rosengreen; I. Brodie Field-emitter arrays for vacuum microelectronics. *IEEE Transactions on Electron Devices* **1991**, *38*, 2355–2363, doi:10.1109/16.88525.
21. Di Bartolomeo, A.; Scarfato, A.; Giubileo, F.; Bobba, F.; Biasiucci, M.; Cucolo, A. M.; Santucci, S.; Passacantando, M. A local field emission study of partially aligned carbon-nanotubes by atomic force microscope probe. *Carbon* **2007**, *45*, 2957–2971, doi:https://doi.org/10.1016/j.carbon.2007.09.049.
22. Di Bartolomeo, A.; Passacantando, M.; Niu, G.; Schlykow, V.; Lupina, G.; Giubileo, F.; Schroeder, T. Observation of field emission from GeSn nanoparticles epitaxially grown on silicon nanopillar arrays. *Nanotechnology* **2016**, *27*, 485707.
23. Iemmo, L.; Di Bartolomeo, A.; Giubileo, F.; Luongo, G.; Passacantando, M.; Niu, G.; Hatami, F.; Skibitzki, O.; Schroeder, T. Graphene enhanced field emission from InP nanocrystals. *Nanotechnology* **2017**, *28*, 495705.
24. Joag, D. S.; More, M. A.; Sheini, F. J. Field Emission from Nanowires. In *Nanowires - Implementations and Applications*; Hashim, A., Ed.; InTech: Rijeka, 2011.
25. Lin, P.-H.; Sie, C.-L.; Chen, C.-A.; Chang, H.-C.; Shih, Y.-T.; Chang, H.-Y.; Su, W.-J.; Lee, K.-Y. Field Emission Characteristics of the Structure of Vertically Aligned Carbon Nanotube Bundles. *Nanoscale Research Letters* **2015**, *10*, 297, doi:10.1186/s11671-015-1005-1.
26. Giubileo, F.; Di Bartolomeo, A.; Scarfato, A.; Iemmo, L.; Bobba, F.; Passacantando, M.; Santucci, S.; Cucolo, A. M. Local probing of the field emission stability of vertically aligned multi-walled carbon nanotubes. *Carbon* **2009**, *47*, 1074–1080, doi:https://doi.org/10.1016/j.carbon.2008.12.035.

27. Di, Y.; Xiao, M.; Zhang, X.; Wang, Q.; Li, C.; Lei, W.; Cui, Y. Large and stable emission current from synthesized carbon nanotube/fiber network. *Journal of Applied Physics* **2014**, *115*, 064305, doi:10.1063/1.4864431.
28. Giubileo, F.; Iemmo, L.; Luongo, G.; Martucciello, N.; Raimondo, M.; Guadagno, L.; Passacantando, M.; Lafdi, K.; Di Bartolomeo, A. Transport and field emission properties of buckypapers obtained from aligned carbon nanotubes. *Journal of Materials Science* **2017**, *52*, 6459–6468, doi:10.1007/s10853-017-0881-4.
29. Di Bartolomeo, A.; Giubileo, F.; Iemmo, L.; Romeo, F.; Russo, S.; Unal, S.; Passacantando, M.; Grossi, V.; Cucolo, A. M. Leakage and field emission in side-gate graphene field effect transistors. *Applied Physics Letters* **2016**, *109*, 023510, doi:10.1063/1.4958618.
30. Suryawanshi, S. R.; More, M. A.; Late, D. J. Exfoliated 2D black phosphorus nanosheets: Field emission studies. *Journal of Vacuum Science & Technology B, Nanotechnology and Microelectronics: Materials, Processing, Measurement, and Phenomena* **2016**, *34*, 041803, doi:10.1116/1.4945433.
31. Giubileo, F.; Di Bartolomeo, A.; Iemmo, L.; Luongo, G.; Passacantando, M.; Koivusalo, E.; Hakkarainen, T. V.; Guina, M. Field Emission from Self-Catalyzed GaAs Nanowires. *Nanomaterials* **2017**, *7*, doi:10.3390/nano7090275.
32. Choi, W. B.; Chung, D. S.; Kang, J. H.; Kim, H. Y.; Jin, Y. W.; Han, I. T.; Lee, Y. H.; Jung, J. E.; Lee, N. S.; Park, G. S.; Kim, J. M. Fully sealed, high-brightness carbon-nanotube field-emission display. *Applied Physics Letters* **1999**, *75*, 3129–3131, doi:10.1063/1.125253.
33. Yabushita, R.; Hata, K.; Sato, H.; Saito, Y. Development of compact field emission scanning electron microscope equipped with multiwalled carbon nanotube bundle cathode. *Journal of Vacuum Science & Technology B: Microelectronics and Nanometer Structures Processing, Measurement, and Phenomena* **2007**, *25*, 640–642, doi:10.1116/1.2429662.
34. Cole, M. T.; Parmee, R. J.; Milne, W. I. Nanomaterial-based x-ray sources. *Nanotechnology* **2016**, *27*, 1–9, doi:10.1088/0957-4484/27/8/082501.
35. Gupta, A. P.; Park, S.; Yeo, S. J.; Jung, J.; Cho, C.; Paik, S. H.; Park, H.; Cho, Y. C.; Kim, S. H.; Shin, J. H.; Ahn, J. S.; Ryu, J. Direct Synthesis of Carbon Nanotube Field Emitters on Metal Substrate for Open-Type X-ray Source in Medical Imaging. *Materials* **2017**, *10*, 878, doi:10.3390/ma10080878.
36. Kong, D.; Wang, H.; Cha, J. J.; Pasta, M.; Koski, K. J.; Yao, J.; Cui, Y. Synthesis of MoS2 and MoSe2 Films with Vertically Aligned Layers. *Nano Letters* **2013**, *13*, 1341–1347, doi:10.1021/nl400258t.
37. Gaur, A. P. S.; Sahoo, S.; Mendoza, F.; Rivera, A. M.; Kumar, M.; Dash, S. P.; Morell, G.; Katiyar, R. S. Cold cathode emission studies on topographically modified few layer and single layer MoS2 films. *Applied Physics Letters* **2016**, *108*, 043103, doi:10.1063/1.4940306.
38. Kashid, R. V.; Late, D. J.; Chou, S. S.; Huang, Y.-K.; De, M.; Joag, D. S.; More, M. A.; Dravid, V. P. Enhanced Field-Emission Behavior of Layered MoS2 Sheets. *Small* **2013**, *9*, 2730–2734, doi:10.1002/smll.201300002.
39. Li, Y. B.; Bando, Y.; Golberg, D. MoS2 nanoflowers and their field-emission properties. *Applied Physics Letters* **2003**, *82*, 1962–1964, doi:10.1063/1.1563307.
40. Sin Ang, Y.; Zubair, M.; Ooi, K. J. A.; Ang, L. K. Generalized Fowler-Nordheim field-induced vertical electron emission model for two-dimensional materials. *arXiv:1711.05898* **2017**.
41. Li, X.; Zhu, H. Two-dimensional MoS2: Properties, preparation, and applications. *Journal of Materiomics* **2015**, *1*, 33–44, doi:https://doi.org/10.1016/j.jmat.2015.03.003.
42. Jariwala, D.; Sangwan, V. K.; Late, D. J.; Johns, J. E.; Dravid, V. P.; Marks, T. J.; Lauhon, L. J.; Hersam, M. C. Band-like transport in high mobility unencapsulated single-layer MoS2 transistors. *Applied Physics Letters* **2013**, *102*, 173107, doi:10.1063/1.4803920.

43. Radisavljevic, B.; Kis, A. Mobility engineering and a metal–insulator transition in monolayer MoS2. *Nature Materials* **2013**, *12*, 815.
44. Amani, M.; Chin, M. L.; Birdwell, A. G.; O'Regan, T. P.; Najmaei, S.; Liu, Z.; Ajayan, P. M.; Lou, J.; Dubey, M. Electrical performance of monolayer MoS2 field-effect transistors prepared by chemical vapor deposition. *Applied Physics Letters* **2013**, *102*, 193107, doi:10.1063/1.4804546.
45. Giubileo, F.; Di Bartolomeo, A. The role of contact resistance in graphene field-effect devices. *Progress in Surface Science* **2017**, *92*, 143–175, doi:https://doi.org/10.1016/j.progsurf.2017.05.002.
46. Xiao, Z.; She, J.; Deng, S.; Tang, Z.; Li, Z.; Lu, J.; Xu, N. Field Electron Emission Characteristics and Physical Mechanism of Individual Single-Layer Graphene. *ACS Nano* **2010**, *4*, 6332–6336, doi:10.1021/nn101719r.
47. Santandrea, S.; Giubileo, F.; Grossi, V.; Santucci, S.; Passacantando, M.; Schroeder, T.; Lupina, G.; Di Bartolomeo, A. Field emission from single and few-layer graphene flakes. *Applied Physics Letters* **2011**, *98*, 163109, doi:10.1063/1.3579533.
48. Choi, S.; Shaolin, Z.; Yang, W. Layer-number-dependent work function of MoS2 nanoflakes. *Journal of the Korean Physical Society* **2014**, *64*, 1550–1555, doi:10.3938/jkps.64.1550.
49. Passacantando, M.; Bussolotti, F.; Santucci, S.; Di Bartolomeo, A.; Giubileo, F.; Iemmo, L.; Cucolo, A. M. Field emission from a selected multiwall carbon nanotube. *Nanotechnology* **2008**, *19*, 395701.
50. Xu, X.; Zhai, T.; Shao, M.; Huang, J. Anodic formation of anatase TiO2 nanotubes with rod-formed walls for photocatalysis and field emitters. *Phys. Chem. Chem. Phys.* **2012**, *14*, 16371–16376, doi:10.1039/C2CP43168H.
51. Fowler and Nordheim Electron emission in intense electric fields. *Proceedings of the Royal Society of London A: Mathematical, Physical and Engineering Sciences* **1928**, *119*, 173–181, doi:10.1098/rspa.1928.0091.